Eurographics Symposium on Rendering - Experimental Ideas & Implementations (2018)
T. Hachisuka and W. Jakob (Editors)

An Improved Multiple Importance Sampling Heuristic for Density Estimates in Light Transport Simulations

J. Jendersie and T. Grosch

TU Clausthal, Germany

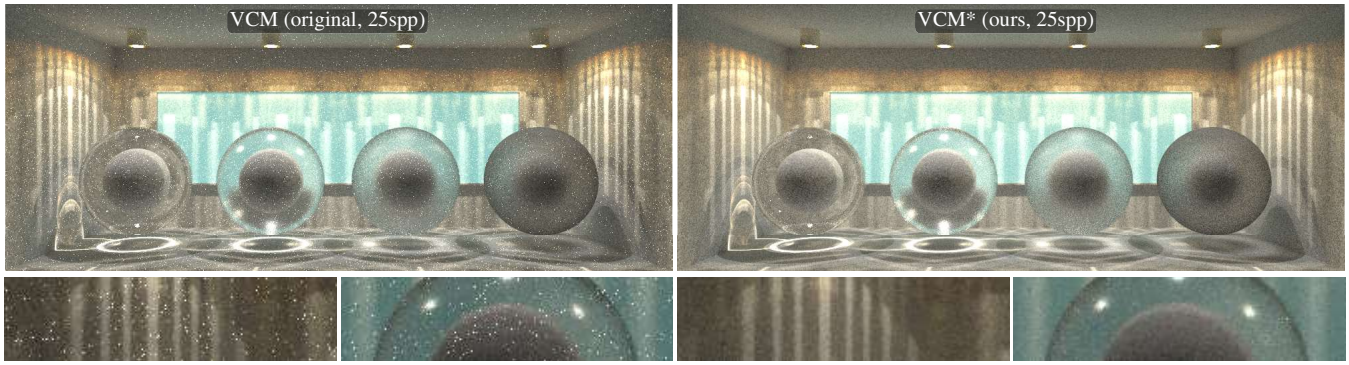

Figure 1: *A scene with glass spheres of varying roughness illuminated by four point lights (placed in highly glossy, faceted cylinders producing striped caustics). Additionally, an area light is used in the background. This scene, having a lot of complex light paths, demonstrates that our heuristic produces less variance than previous methods, robustly. The darkened (-2EV) closeups demonstrate the HDR nature of noise pixels in the original VCM technique.*

Abstract

Vertex connection and merging (VCM) is one of the most robust light transport simulation algorithms developed so far. It combines bidirectional path tracing with photon mapping using multiple importance sampling (MIS). However, there are scene setups where the current weight computation is not optimal. If different merge events on a single path have roughly the same likelihood to be found, but different photon densities, this leads to high variance samples.

We show how to improve the heuristic for density estimation events to overcome this issue by including the photon density into the MIS computation. This leads to a faster convergence in VCM and related techniques. The proposed change is easy to implement and is orthogonal to other improvements of the algorithm.

CCS Concepts

•***Computing methodologies*** → *Ray tracing;* •***Mathematics of computing*** → ***Sequential Monte Carlo methods;***

1. Introduction

In recent years, with stronger hardware, Monte Carlo light transport simulation got more and more attention in production rendering. The scenes become ever more complex with respect to geometry and materials. The latter leads to an increasing number of complex light situations where one integration technique may fail and another may succeed.

One such technique, Bidirectional Path Tracing (BPT) [VG95, LW93], connects paths from the light sources and the observer. All different possibilities to create a certain path are weighted based on their path probabilities as described in Section 3. BPT can handle caustics (via light tracing) and mirrors/glass objects (via importance tracing) well. However, it has severe problems with SDS (specular-diffuse-specular) paths which cannot be sampled by any of the connection strategies.

Photon Mapping [Jen96] finds SDS paths well, introducing a small bias, but is difficult to combine with bidirectional path tracing. Georgiev et al. [GKDS12] and Hashisuka et al. [HPJ12] both derived the same unified weight function for photon mapping which is compatible with BPT.

DOI: 10.2312/sre.20181173

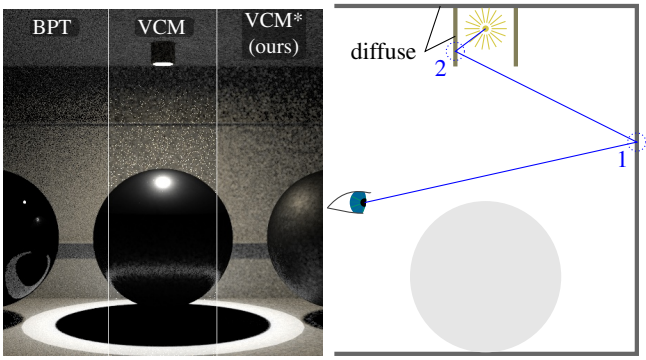

Figure 2: *An example for path length three with simple diffuse bounces and a point light source (50spp). VCM weights both possible merges (1,2) with roughly the same weight. Our approach prefers connection paths and the merge at 1.*

While the VCM heuristic is correct for single path merges without reuse, it fails for some cases once we merge with multiple light paths. For an example see Figure 2, in which VCM has an even higher variance than BPT. This shows us that at least one merge with an actual higher variance than the connection paths is now overestimated in its importance. More specific, this happens for the merge at vertex 2 in the schematic sketch. Since the variance of the merge at vertex 2 is mainly caused by the view sub-path, increasing the photon count will not decrease the variance by the number of photons. This means that increasing the path reuse will not decrease the variance linearly at all merge points. However, in VCM both alternatives have roughly the same probability (by construction of the example) and are weighted equally. The *balance heuristic* in VCM multiplies the total number of photons with the probability for all merges which causes an overestimation of some merge-path probabilities.

We propose a new heuristic in Section 5 which includes the photon density to find a more robust solution which *shifts the merges towards the viewer*. The difference to the previous weighting in [GKDS12, HPJ12] is a change in the photon gathering acceptance probability p_{acc}, only. This allows an easy integration in existing VCM renderers and related techniques like [ŠOHK16].

2. Related Work

As explained, we base our work on Veach's foundation for BPT [Vea97] and the extension to include photon mapping in [GKDS12] and [HPJ12]. The original Photon Mapping [Jen96] gathers photons from a search data structure within a small radius around the current hit point to compute the local illumination. A problem with this approach is its bias. It blurs light according to the query radius and may even produce light bleeding artifacts. Progressive Photon Mapping [HOJ08] solves this problem by reducing the query radius over time. To accomplish that, a statistics per path-end-point is recorded such that the number of photons in the gathering event can be kept constant. To track the statistics only a single path per pixel is used which also results in aliasing. Stochastic Progressive Photon Mapping (SPPM) [HJ09] uses new view-paths every iteration and shares the statistics within a pixel. It allows a broader range of effects like depth of field and is able to avoid aliasing. Knaus and Zwicker [KZ11] showed that a single global radius, which decreases over the iterations, is sufficient for convergence. We use their approach in the photon mapping part of our implementation.

Besides random connections (BPT) and merging (SPPM), another class of samplers exists. Markov Chain Monte Carlo (MCMC), also introduced by Veach [VG97], explores the path space by conditionally accepting path mutations. In [ŠOHK16] MCMC is combined with VCM. This method should benefit from our new heuristic, too.

Another related technique is Unbiased Photon Gathering (UPG) [QSH*15] which uses a random trial process to determine the bias of a photon gathering event in VCM. They modify the merge acceptance probability p_{acc}, like our method, but with a different objective. It is still possible for UPG to have a high variance (e.g. in Figure 2). On the other hand, our method does not force a bias reduction. We propose a variant of our modification (VCM+) which penalizes bias to some degree, but which cannot provide the guarantees of UPG. It is possible to combine both modifications to get our robustness and UPG's unbiasedness.

A method to estimate an error bound of merge events is given by Hachisuka et al. [HJJ10]. They apply the derived bound to adaptively stop the rendering after reaching a sufficient small error confidently. Similarly, Kaplanyan and Dachsbacher [KD13] use an error bound to adaptively set the radius of a merge event. Both target to reduce the error (bias+variance) of a given radiance estimate. We show that, in VCM-like techniques, it is also of high importance to select the merge points correctly, to avoid high variance cases. It is still possible to apply adaptive radii or rendering stop criteria for all of the merges on a path to reduce the error.

Our method solely reduces the variance by choosing the sampler more robustly. It still benefits from other variance reduction techniques like Adjoint driven Russian Roulette and Splitting [VK16] and guidance methods [HEV*16,MGN17]. All three techniques require additional data for the spatial and angular varying adjoint quantities (light and importance). We also use an additional density map which could be combined with the guidance structures to reduce the memory and performance overhead in a combined method.

3. Multiple Importance Sampling Reviewed

Multiple importance sampling (MIS) is a general framework in the context of Monte Carlo integration. It weights samples, drawn from different probability distributions p, to get a low variance combination. The chosen heuristic can have a large impact on the variance as shown in the survey [EMLB17] and Veach's thesis [Vea97]. The general form used in light transport algorithms is

$$w_i = \frac{(n_i p_i)^\beta}{\sum_k (n_k p_k)^\beta}, \tag{1}$$

where the weight w_i for sample i depends on the probabilities of all sampling techniques p_k and the numbers n_k of samples drawn from that distributions. β can be used to amplify the choice of certain techniques. Using $\beta = 1$ is called the *balance heuristic* which we use in this work. In all cases, the weights w_i sum up to 1.

3.1. MIS in Bidirectional Techniques

In BPT the probabilities p from Eq. (1) for the different path sampling strategies are defined as

$$p_{C,i} = p(x_1) \cdot \prod_{j=1}^{i-1} p(x_j \to x_{j+1}) \cdot \prod_{j=i+1}^{\ell-1} p(x_j \leftarrow x_{j+1}) \cdot p(x_\ell). \quad (2)$$

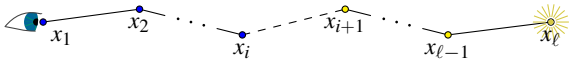

The probability of a path consists of the probabilities of the two sub-paths. The full path has ℓ vertices from which $\ell - i$ vertices belong to the light sub-path. $\overrightarrow{p}(x_\ell)$ is the probability to sample the light source which is not used in the unidirectional path tracing case $i = \ell$. The view sub-path has $i \geq 1$ vertices. Here, usual implementations do not support a random hit of the camera (i.e. $i = 0$) and for a single camera $p(x_1) = 1$ is set. All different sampling alternatives for the path have the same length ℓ, but differ in the partition position i of the connection vertex.

The probabilities of individual segments in the random walk are computed with respect to the area measure

$$p(x_j \to x_{j+1}) = \frac{\overrightarrow{p}(x_j) |\cos\theta_{j \to j+1}|}{\|x_j - x_{j+1}\|^2},$$

where $\theta_{j \to j+1}$ is the angle between normal and incident direction at vertex x_{j+1} and $\overrightarrow{p}(x_j)$ is the sampling PDF used to sample the excident direction. The result is a probability density per unit area, i.e. the chance to hit this surface point using the given sampler. The probability in the reversed direction $p(x_j \leftarrow x_{j+1})$ is defined analogously with replaced directions and indices. Note that $\overrightarrow{p}(x_j) \neq \overleftarrow{p}(x_j)$ in general.

3.2. Extension for Photon Mapping

In photon mapping, additional paths are found by performing a search in the local neighborhood of the end point of one of the sub-paths (merge event).

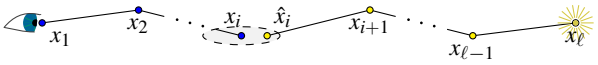

Unfortunately, these paths have one additional vertex and are not comparable to the connection-based paths directly. A solution was proposed by Georgiev et al. [GKDS12] and Hachisuka et al. [HPJ12] at the same time: Instead of the probability $p(\hat{x}_i \leftarrow x_{i+1})$ with unit m^{-2}, the unitless probability for a merge event p_{acc} is used.

$$p_{\text{acc}}(x_i) = \int_{\mathcal{A}} p(x_i \leftarrow x_{i+1}) \mathrm{d}x \quad (3)$$
$$\approx |\mathcal{A}| p(\hat{x}_i \leftarrow x_{i+1}) = \pi r^2 p(\hat{x}_i \leftarrow x_{i+1})$$

is the integral over the surface patch at the merge event. Its approximation uses only one sample of $p(x_i \leftarrow x_{i+1})$, i.e. the known segment probability, and the area of a disc with the user-specified query radius r. According to [GKDS12] this approximation converges to the true result if r is decreased over time and works well in practice.

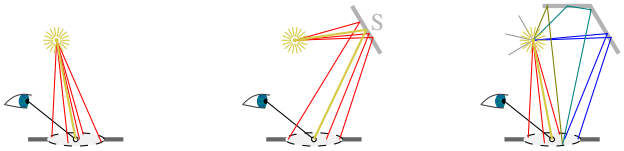

Figure 3: *Examples of paths (red) which become identical (yellow) through a merge by setting $\hat{x}_i := x_i$. Left: Direct light. Middle: A specular bounce behaves equal to direct light. Right: Total number of $n_\Phi = 10$ emitted photons from which $k = 7$ reached the gathering region. The gathered photons correspond to independent path sets, where only $m = 3$ belong to the direct light sub-path.*

By using Eq. (3) we obtain the final path probability for merge paths

$$p_{M,i} = p_{C,i} \cdot \pi r^2 p(\hat{x}_i \leftarrow x_{i+1}) \quad (4)$$

This probability is correct for a single light sub-path. However, the true strength of VCM lies in its path reuse (see [GKDS12] for an example). If we reuse a high number of photons n_Φ, the current solution is to multiply $p_{M,i}$ with n_Φ in the context of Eq. (1). This scalar multiplication is applied to each merge event equally, which causes the invalid decisions as described in the introduction.

4. Probability of Merge Paths with Respect to Reuse

By using $n_\Phi \cdot p_M$ in the *balance heuristic* Eq. (1) the likeliest sampler should be preferred. However, there are scenes for which even plane BPT results in a lower variance for some paths (consider the example of Figure 2). Seemingly, a merge path with a higher variance than one of the connection paths is chosen in this case. Thus, the effective reuse of paths must be overestimated.

Without formal introduction let f be the *path measurement contribution* function [Vea97, p. 222] which is deterministic for a path given all its vertices. Each of two or more merge events on the same path are computing a Monte-Carlo sample $f/p^*_{M,i}$ of the same and constant quantity f, where $p^*_{M,i} = c_i p_{M,i}$ includes the unknown factor $c_i \in [1, n_\Phi]$ for the reuse advantage. Without path reuse these merge events will either happen or not and by setting $c_i = 1$ we have the required probability for these samples.

If n_Φ photons are sent and reused the behavior will change. A single merge can now find many similar light sub-paths. Figure 3 gives examples for which multiple paths (red) are identical after merging. It also shows that this effect is not limited to direct lighting. Longer paths can still have multiple identical sub-paths, although they diverged up to the query area. This applies to non-specular bounces in a similar way.

To find the appropriate factor c_i, let us begin with the contribution to a pixel's radiance estimate, computed by a merge event:

$$\frac{W(x_1)}{p(x_1)} \prod_{h=2}^{i-1} \frac{\rho(x_h)}{p(x_h)} \cdot \sum_{j=1}^{k} \left[\frac{\rho_j(x_i)}{\pi r^2} \cdot \left(\prod_{h=i+1}^{\ell_j - 1} \frac{\rho(x_{h,j})}{p(x_{h,j})} \right) \cdot \frac{L_e(x_{\ell,j})}{p(x_{\ell,j})} \right] \quad (5)$$

where L_e is the emitted radiance at the light source, W is the sensor response, $\rho(x_h)$ the reflectance (BSDF) at the intermediate vertices and k the number of photons found in the merge region.

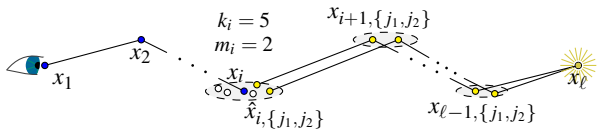

In equation (5) the k light sub-paths may be different or identical paths. Let $\widetilde{m}_i \in [0, n_\Phi]$ be the expected number of equivalent paths which are found in the merge at vertex i as described above (only diverging up to the merge radius). Note that $\widetilde{m}_i$ is not necessarily an integral number, rather it is the average of observed equivalent paths m_i over an infinite number of iterations. Since all these paths are treated as identical from the merge we can set them equal and replace the sum over these paths by a product

$$M_i = \frac{W(x_1)}{p(x_1)} \cdot \left(\prod_{h=2}^{i-1} \frac{\rho(x_h)}{p(x_h)} \right) \cdot \widetilde{m}_i \cdot \frac{\rho(x_i)}{\pi r^2} \cdot \left(\prod_{h=i+1}^{\ell-1} \frac{\rho(x_h)}{p(x_h)} \right) \cdot \frac{L_e(x_\ell)}{p(x_\ell)}.$$

We know that M_i is an estimate of $f/p^*_{\mathrm{M},i}$ and $M_j = f/p^*_{\mathrm{M},j}$ for a different merge vertex j in the same way. By dividing the two equations we have

$$\begin{aligned}
& \frac{f/p^*_{\mathrm{M},i}}{f/p^*_{\mathrm{M},j}} = \frac{M_i}{M_j} \\
\Leftrightarrow \quad & \frac{p^*_{\mathrm{M},j}}{p^*_{\mathrm{M},i}} = \frac{W(x_1) \cdot \widetilde{m}_i \cdot \prod_{h=2}^{\ell-1} \rho(x_h) \cdot L_e(x_\ell)}{W(x_1) \cdot \widetilde{m}_j \cdot \prod_{h=2}^{\ell-1} \rho(x_h) \cdot L_e(x_\ell)} \cdot \frac{p_{\mathrm{M},j}}{p_{\mathrm{M},i}} \\
\Leftrightarrow \quad & \frac{p^*_{\mathrm{M},j}}{p^*_{\mathrm{M},i}} = \frac{\widetilde{m}_i \cdot p_{\mathrm{M},j}}{\widetilde{m}_j \cdot p_{\mathrm{M},i}} = \frac{c_j \cdot p_{\mathrm{M},j}}{c_i \cdot p_{\mathrm{M},i}} \\
\Leftrightarrow \quad & \frac{\widetilde{m}_i}{\widetilde{m}_j} = \frac{c_j}{c_i}.
\end{aligned}$$

In the second line we rearranged the terms using the known $p_{\mathrm{M},i}$ from Eq. (4). Most of the terms are identical for both paths and cancel out in the third line. As a result we obtain $c_i \propto 1/\widetilde{m}_i$ as the searched weight.

How is this connected with the variance of the random walk in the view sub-path? If using a good importance sampler close to the BSDF, the variance of the sampling is almost zero. Therefore, the increase in variance primarily originates in the distribution of incoming radiance, which depends on the density of photons. Thus we can use the numbers $\widetilde{m}_i$ to derive a new factor $c_i \in [1, n_\Phi]$ instead of using $c_i = n_\Phi$ as in the original VCM.

5. A New Improved Heuristic

In practice we did one simplification to arrive at a feasible solution. Instead of using the expected number of equal paths $\widetilde{m}_i$ we use the average number of all photons $\tilde{k}_i > \widetilde{m}_i$ found in the merge region, because $\widetilde{m}_i$ is much harder to compute. As an intermediate result we obtain the heuristic for VCM$^+$

$$c_i^+ = \frac{n_\Phi}{\tilde{k}_i} \tag{6}$$

which already models the shift of merges towards the viewer, but lacks normalization when comparing to connections.

The overestimation of $\widetilde{m}_i$ by using $\tilde{k}_i$ is the main reason why there are situations for which the original VCM is better than VCM$^+$. Examples are shown in Figure 6.

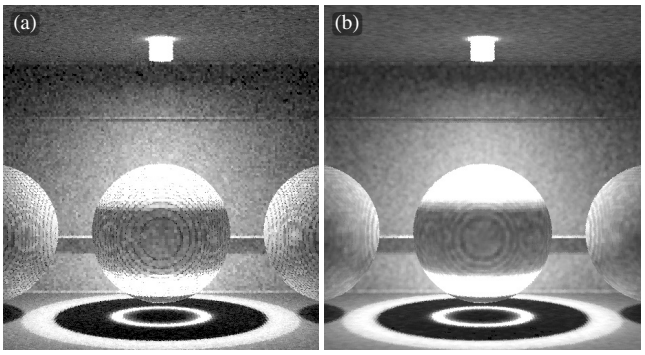

Figure 4: *Nearest point sampling (a) and a custom 2^3 filter (b) applied to the density map after 50 iterations. The scene is that from Figure 2 but with unrestricted path length.*

We found experimentally that dividing by the average of $1/\tilde{k}_i$ over all possible merges along the path gives a more robust solution. This normalization restores the weight between connection and merge paths to that of VCM while the shift between merges remains. It thus decreases the effect of photons from other paths.

The final weight we use for VCM* is

$$c_i^* = \frac{n_\Phi}{\tilde{k}_i} \cdot \left(\frac{1}{\ell - 2} \sum_{j=2}^{\ell-1} \frac{1}{\tilde{k}_j} \right)^{-1}, \tag{7}$$

for which the $\tilde{k}_j$ along the path are obtained from an additional data structure described in the next section.

5.1. The Density Map (DM)

The overall goal of the density map is to deliver queries of $\tilde{k}_i$ fast for any position x. Since it is used to improve the MIS heuristic only, we can accept biased results from the density map itself.

It is possible to use the already existing photon map to find the number of merges as an approximation to the integral. However, this has two disadvantages: performance and variance of the MIS weight computation. Dependent on the type of the photon map this comes with a different performance penalty. Our implementation uses a hash grid including all photons (collisions are resolved using linked lists as in [JRBG17]). This leads to a query time of $\mathcal{O}(k)$ for k being the number of photons in the hash-cell. Alternatively, if a stochastic hash grid [HJ10] is used, the query time is $\mathcal{O}(1)$, but in this case the renderer variance increases due to stochastic collision handling. We therefore introduce the independent density map and stick to the non-stochastic version of a photon map.

With respect to the second disadvantage, a dedicated data structure allows us to decrease the variance in the weight computation by accumulating the count over time. Other than for photons this does not increase memory requirements. Accumulation leads to a convergence of the DM which even allows to disable the insertion of new photons after some iterations (we used 50 in our experiments). Afterwards, the samples of $\tilde{k}_i$ are deterministic and the requirement for an unbiased MIS [Vea97] holds.

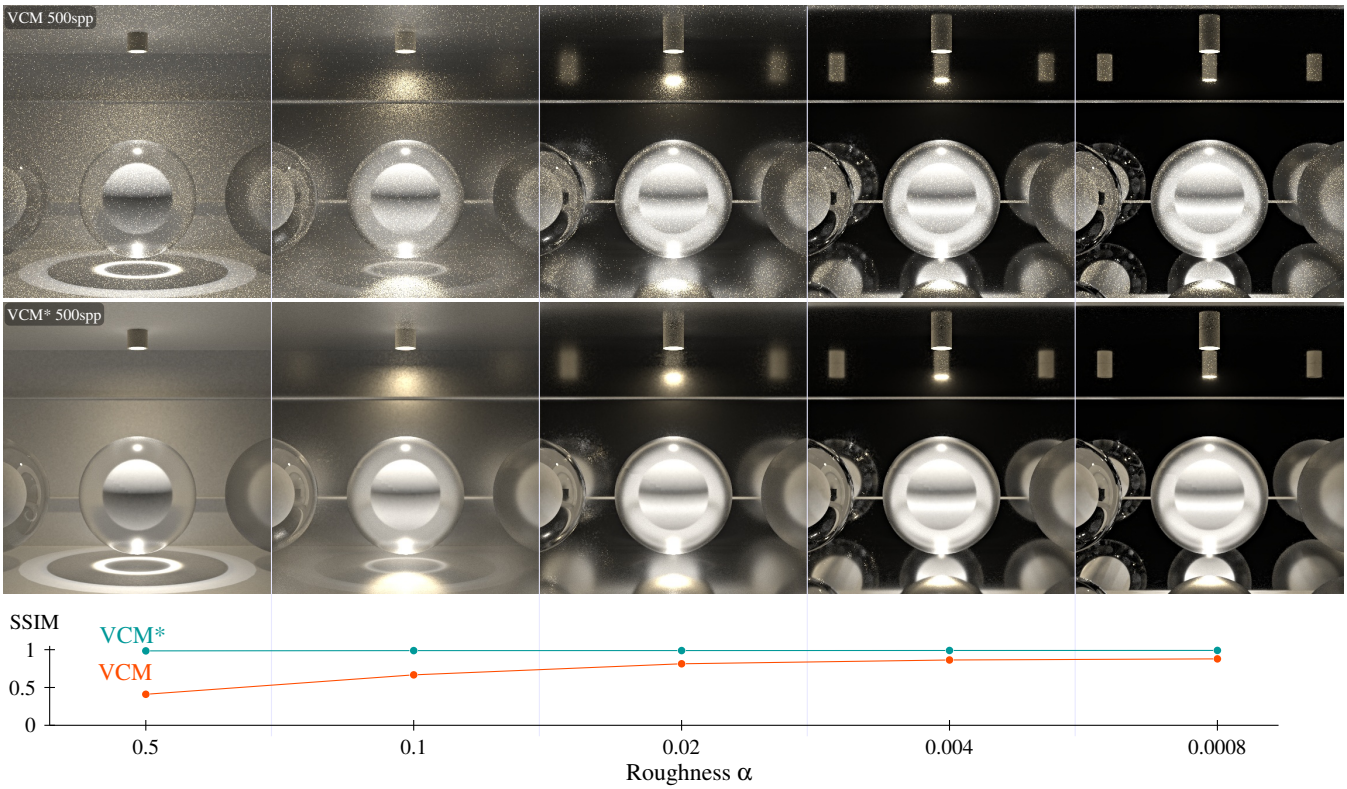

Figure 5: *Robustness of VCM* over varying BSDFs. The negative impact of the merge overestimation in VCM (top row) applies even for very smooth surfaces. Our VCM* solves this problem over a wide range of parameters and paths. Only merges on the outside of the cylinder are over-penalized, because the DM leaks photons from the inside as visible in Figure 4.*

To implement the DM we use, again, a hash grid, where we simply count the number of collisions in each cell instead of adding data entries. Figure 4 visualizes the content of the DM after 50 iterations. The filtered version uses the 8 neighbors also used in bilinear filtering, but ignores samples for which the count is zero. I.e. the sum of all counts multiplied with a weight is divided by the sum of weights for cells with a count greater zero. This is important, because we try to integrate over a surface, but use cells from a volume. Consequently, there are always empty cells which must be ignored. For the weight we used $w_c = e^{-\|x-x_c\|}$ as a radial base function dependent on the distance between cell center x_c and sampling position x.

Sampling the DM yields the number of photons q integrated over the cell region r_c^2 over all iterations n_{it}. To convert this into the number of photons inside the query area πr^2 we must compute

$$\tilde{k} = q \cdot \pi r^2 / (r_c^2 \cdot n_{\text{it}}).$$

The cell area r_c^2 is an approximation of the true area of geometry in this cell. It holds for axis aligned planar surfaces and is an approximation otherwise.

One remaining issue is that the photon count in a cell q can be zero in low density regions. This would cause a division by zero in equations (6) and (7). On the other hand the true average of photons cannot be zero in regions with valid transport paths. Thus, we introduce the regularization $q' = \max(q, 1/n_{\text{it}})$ over the iterations. For a low average region the expected value is one photon in $1/q$ iterations. So, q' models the expected observable count.

6. Results

Validity: While we made several simplifications – most of all using the too big number of photons $\tilde{k}_i$ – VCM* (using Eq. (7)) is superior to VCM in all tested scenes. Figure 5 demonstrates the robustness over different glossy paths while Figure 6 and the supplemental show a broad range of different scenes. Thus, decreasing the expected effect of path reuse by the connected photon density improves the robustness of VCM-like algorithms.

Quality: Besides the constructed examples (Teaser 1, Figure 2) which naturally converge faster, we also tested the convergence for different scenes shown in Figure 6. A more complete visual comparison is given in the supplemental. The plots on the right side show the convergence for the first 1024 iterations with respect to various metrics:

RMSE	SRRMSE	SSIM
$\sqrt{\frac{1}{N}\sum_i^N (x_i - r_i)^2}$	$\sqrt{\frac{1}{N}\sum_i^N \left[\frac{x_i - r_i}{(x_i + r_i)/2}\right]^2}$	$\frac{(2\mu_{xi}\mu_{ri} + C_1)(2\sigma_{xri} + C_2)}{(\mu_{xi}^2 + \mu_{ri}^2 + C_1)(\sigma_{xi}^2 + \sigma_{ri}^2 + C_2)}$

Here, x_i and r_i are the ith-pixel value of the image and the reference image and μ, σ are local statistics at each pixel. For more

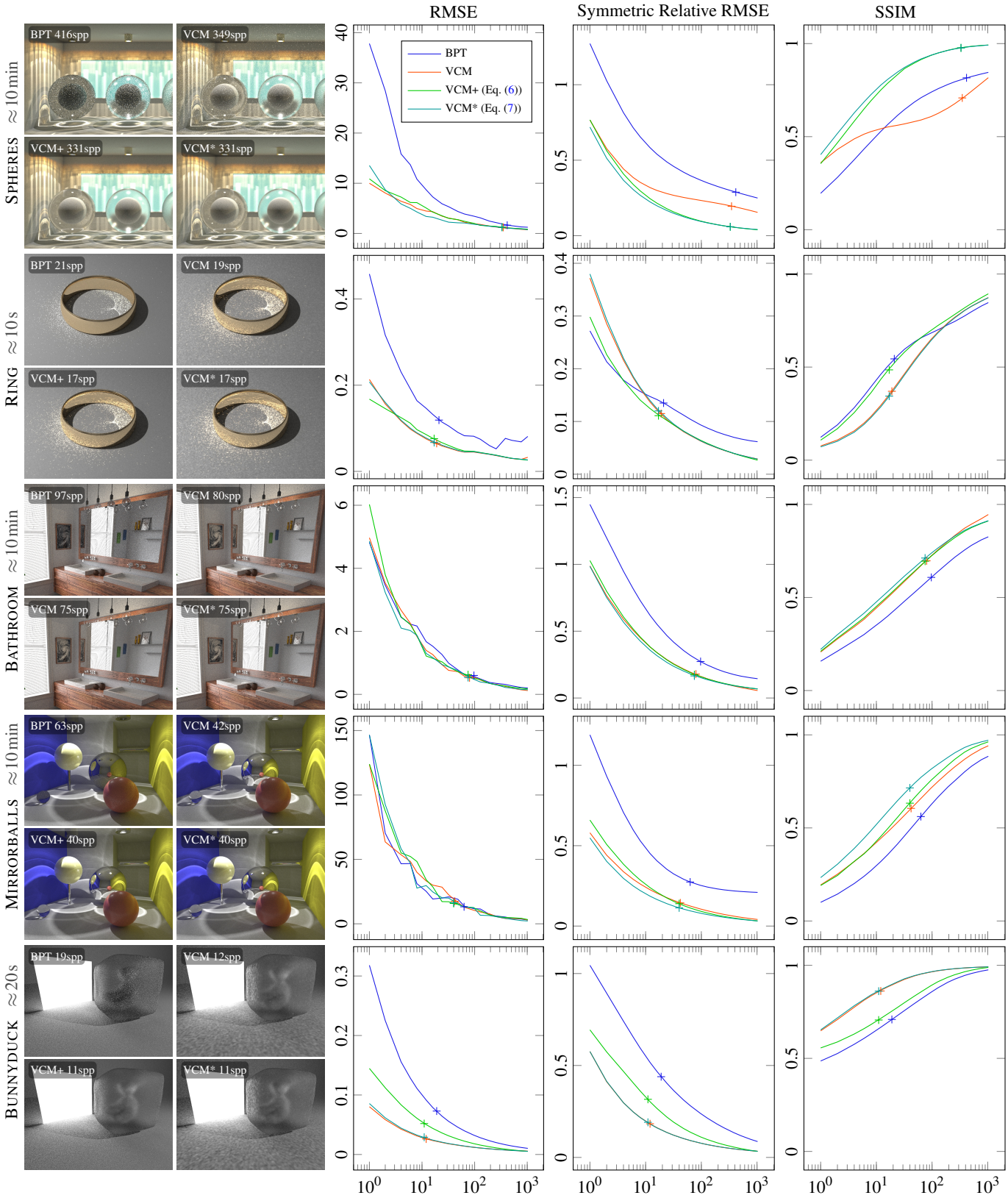

Figure 6: *Convergence plots and equal time example images for a subset of scenes. The markers denote the iteration/error of the shown images. Due to equal time comparison the images are from different iterations. Uncropped image series and more scenes can be found in the supplemental material.*

details on structured similarity (SSIM) and the constant values C_1 and C_2 please refer to [WBSS04]. For the reference images we used VCM* with over 12000 iterations (4h-12h).

The Root Mean Squared Error (RMSE) is often noisy due to high variance specular paths and makes a comparison between the VCM variants difficult. It shows that BPT clearly has a higher variance for most of the scenes, but even fails to detect the missing SDS paths in the MIRRORBALLS scene.

The two other plots show more perception-based measures: Symmetric Relative RMSE (SRRMSE) which weights over- and under-estimations the same and SSIM which was explicitly designed as a perception-based measure.

In almost all cases VCM* is at least as good, but often better, than standard VCM. There is an exception in the BATHROOM scene where SSIM shows an increased error on the right side. Our variant VCM* prefers merges on the infacing roller blind sides instead of the outfacing ones. Due to light-bleeding within the merge radius these have a higher bias. Both methods are still consistent and will converge to the same result.

In some scenes (BUNNYDUCK and RING) results are slightly worse than for the original VCM. This happens, because using $\tilde{k}_i$ in these scenes is a significant mis-evaluation of the required quantity. In the RING scene the bright caustic and the direct light both contribute many photons while being totally different paths. In the BUNNYDUCK scene direct light from the point light and the area light overlay in a similar way.

Comparing VCM+ to the other methods, it mixes characteristics of VCM* and BPT. In scenes where VCM fails, VCM+ is more robust (SPHERES, Supplemental: VEACH, DOUBLEMERGE, DRAGON). However, it has a higher variance due to over-penalizing merges. This can be an advantage, if the error mainly depends on bias (e.g. RING scene).

Performance: For the hash grid we allocated 16 M integer counters which resulted in only 64 MB additional memory requirement.

The increase in computation time is between 15% and 20% with respect to the total rendering time. The influence is smaller in more complex scenes, because tracing costs in those scenes is higher. Also, implementing a lock-free hash grid would roughly half the cost. We experimented with a variant, which increased computation time by only 5% to 9%, but had several artifacts on its own.

7. Conclusions

We have shown that current multiple importance sampling for VCM and similar techniques is not optimal with respect to variance. It may overestimate the importance of some merge events leading to well visible noise. We incorporated the photon density to the path probability to solve this problem. Our new heuristic leads to a more robust version of VCM producing better or equally good results than the previous version.

7.1. Future Work

One problem of our method is the requirement of an additional data structure. However, if combined with one of the guidance methods (e.g. [VK16,HEV*16,MGN17]) the density could be gathered from the existing information. Also, it could be possible to reduce the query times for the density by perfect spatial hashing [LH06].

An improvement to the reliability and quality can be expected if $\tilde{m}_i$ instead of $\tilde{k}_i$ could be evaluated. This could be done by increasing the dimensionality of the hash grid. Using the union of all path vertices (i.e. 3 dimensions per vertex) would separate all paths which diverge more than the cell size in any vertex.

Another avenue is to find a different analytic description which directly uses the view sub-path probability to decide about the variance reduction of reuse at each of its vertices.

Finally, a combination with UPG [QSH*15] would be interesting as both modifications target different problems of the merge events. The combined result would be unbiased and more robust at the same time.

7.2. Acknowledgments

We thank all the anonymous reviewers and Andreas Reich for their objections which helped us to improve our own understanding of the problem. Further, we want to thank those who made their test scenes publicly available. We took many scenes (VEACH-BIDIR, BATHROOM, VILLA, DRAGON) from the PBRT-repository [PJH17] and the MIRRORBALLS scene from [Vev18] with special thanks to Toshiya Hachisuka who modeled the original scene.

References

[EMLB17] ELVIRA V., MARTINO L., LUENGO D., BUGALLO M. F.: Generalized Multiple Importance Sampling. *arXiv:1511.03095v2* (2017). URL: https://arxiv.org/abs/1511.03095v2. 2

[GKDS12] GEORGIEV I., KŘIVÁNEK J., DAVIDOVIČ T., SLUSALLEK P.: Light Transport Simulation with Vertex Connection and Merging. *ACM Transactions on Graphics (Proc. of SIGGRAPH Asia) 31*, 6 (2012), 192:1–192:10. URL: http://doi.acm.org/10.1145/2366145.2366211. 1, 2, 3

[HEV*16] HERHOLZ S., ELEK O., VORBA J., LENSCH H., KŘIVÁNEK J.: Product Importance Sampling for Light Transport Path Guiding. *Computer Graphics Forum (CGF) 35*, 4 (2016), 67–77. URL: http://dx.doi.org/10.1111/cgf.12950. 2, 7

[HJ09] HACHISUKA T., JENSEN H. W.: Stochastic Progressive Photon Mapping. *ACM Transactions on Graphics (TOG) 28*, 5 (Dec. 2009), 141:1–141:8. URL: http://doi.acm.org/10.1145/1618452.1618487. 2

[HJ10] HACHISUKA T., JENSEN H. W.: Parallel Progressive Photon Mapping on GPUs. In *ACM SIGGRAPH Asia Sketches* (2010), ACM, p. 54. URL: http://doi.acm.org/10.1145/1899950.1900004. 4

[HJJ10] HACHISUKA T., JAROSZ W., JENSEN H. W.: A Progressive Error Estimation Framework for Photon Density Estimation. *ACM Transactions on Graphics (Proc. of SIGGRAPH Asia) 29*, 6 (Dec. 2010), 144:1–144:12. URL: https://cs.dartmouth.edu/~wjarosz/publications/hachisuka10progressive.html. 2

[HOJ08] HACHISUKA T., OGAKI S., JENSEN H. W.: Progressive Photon Mapping. *ACM Transactions on Graphics (TOG) 27 number 5* (2008), 130. URL: http://doi.acm.org/10.1145/1409060.1409083. 2

[HPJ12] HACHISUKA T., PANTALEONI J., JENSEN H. W.: A Path Space Extension for Robust Light Transport Simulation. *ACM Transactions on Graphics (Proc. of SIGGRAPH Asia) 31*, 6 (Nov.

2012), 191:1–191:10. URL: http://doi.acm.org/10.1145/2366145.2366210. 1, 2, 3

[Jen96] JENSEN H. W.: Global Illumination using Photon Maps. In *Proc. of Eurographics Workshop on Rendering (EGWR)* (1996), Springer, pp. 21–30. URL: http://dl.acm.org/citation.cfm?id=275458.275461. 1, 2

[JRBG17] JENDERSIE J., ROHMER K., BRÜLL F., GROSCH T.: Pixel Cache Light Tracing. In *Proc. Vision, Modeling and Visualization (VMV)* (2017), pp. 137–144. URL: http://diglib.eg.org/handle/10.2312/vmv20171269. 4

[KD13] KAPLANYAN A. S., DACHSBACHER C.: Adaptive Progressive Photon Mapping. *ACM Transactions on Graphics (TOG) 32*, 2 (Apr. 2013), 16:1–16:13. URL: http://doi.acm.org/10.1145/2451236.2451242. 2

[KZ11] KNAUS C., ZWICKER M.: Progressive Photon Mapping: A Probabilistic Approach. *ACM Transactions on Graphics (TOG) 30*, 3 (2011), 25. URL: http://doi.acm.org/10.1145/1966394.1966404. 2

[LH06] LEFEBVRE S., HOPPE H.: Perfect Spatial Hashing. *ACM Transactions on Graphics (Proc. SIGGRAPH) 25*, 3 (July 2006), 579–588. URL: http://doi.acm.org/10.1145/1141911.1141926. 7

[LW93] LAFORTUNE E. P., WILLEMS Y. D.: Bi-Directional Path Tracing. In *Proc. of Conference on Computational Graphics and Visualization Techniques* (1993), pp. 145–153. URL: https://lirias.kuleuven.be/handle/123456789/132773. 1

[MGN17] MÜLLER T., GROSS M., NOVÁK J.: Practical Path Guiding for Efficient Light-Transport Simulation. In *Proc. of Eurographics Symposium on Rendering (EGSR)* (June 2017). URL: http://onlinelibrary.wiley.com/doi/10.1111/cgf.13227/full. 2, 7

[PJH17] PHARR M., JAKOB W., HUMPHREYS G.: *Physically Based Rendering: From Theory to Implementation*, 3 ed. Morgan Kaufmann, 2017. URL: http://www.pbrt.org/. 7

[QSH*15] QIN H., SUN X., HOU Q., GUO B., ZHOU K.: Unbiased Photon Gathering for Light Transport Simulation. *ACM Transactions on Graphics (TOG) 34*, 6 (2015), 208:1–208:14. URL: http://doi.acm.org/10.1145/2816795.2818119. 2, 7

[ŠOHK16] ŠIK M., OTSU H., HACHISUKA T., KŘIVÁNEK J.: Robust Light Transport Simulation via Metropolised Bidirectional Estimators. *ACM Transaction on Graphics (TOG) 35*, 6 (2016), 245:1–245:12. URL: http://doi.acm.org/10.1145/2980179.2982411. 2

[Vea97] VEACH E.: *Robust Monte Carlo Methods for Light Transport Simulation*. PhD thesis, Stanford University, 1997. URL: http://graphics.stanford.edu/papers/veach_thesis/. 2, 3, 4

[Vev18] VEVODA P.: Small UPBP Repository, 2018. URL: https://github.com/PetrVevoda/smallupbp/tree/master/scenes/mirrorballs. 7

[VG95] VEACH E., GUIBAS L. J.: Bidirectional Estimators for Light Transport. In *Photorealistic Rendering Techniques*. Springer Berlin Heidelberg, 1995, pp. 145–167. URL: http://dx.doi.org/10.1007/978-3-642-87825-1_11. 1

[VG97] VEACH E., GUIBAS L. J.: Metropolis Light Transport. In *Proceedings of SIGGRAPH '97* (1997), pp. 65–76. URL: http://dx.doi.org/10.1145/258734.258775. 2

[VK16] VORBA J., KŘIVÁNEK J.: Adjoint-Driven Russian Roulette and Splitting in Light Transport Simulation. *ACM Transactions on Graphics (TOG) 35*, 4 (2016), 1–11. URL: http://doi.acm.org/10.1145/2897824.2925912. 2, 7

[WBSS04] WANG Z., BOVIK A. C., SHEIKH H. R., SIMONCELLI E. P.: Image Quality Assessment: from Error Visibility to Structural Similarity. *IEEE Transactions on Image Processing (TIP) 13*, 4 (2004), 600–612. URL: https://doi.org/10.1109/TIP.2003.819861. 7